IASMiRT

SMiRT 26
50 Anniversary Berlin/Potsdam

Transactions, SMiRT-26
Berlin/Potsdam, Germany, July 10-15, 2022
Division I

DEPENDENCE OF DEFORMATION AND FRACTURE PROPERTIES OF STEELS ON STRAIN RATE, STRESS TRIAXIALITY AND TEMPERATURE

Tomohisa Kumagai[1], Hayato Tokunaga[2], Yoshiki Tsunemoto[2], Masato Yamamoto[3], Naoki Miura[4], Junmin Seo[5], Yun-Jae Kim[6], Hidekazu Takazawa[7], Hiroyuki Yamada[8].

[1] Senior Research Scientist, Central Research Institute of Electric Power Industry, Yokosuka, Kanagawa, Japan. (kumagai@criepi.denken.or.jp)
[2] Research Associate, Central Research Institute of Electric Power Industry, Yokosuka, Kanagawa, Japan.
[3] Senior Research Scientist, Central Research Institute of Electric Power Industry, Yokosuka, Kanagawa, Japan.
[4] Distinguished Research Scientist, Central Research Institute of Electric Power Industry, Yokosuka, Kanagawa, Japan.
[5] Ph. D student, Korea University, Seoul, Korea.
[6] Professor, Korea University, Seoul, Korea.
[7] Ph.D student, National Defence Academy of Japan, Yokosuka, Kanagawa, Japan.
[8] Associate Professor, National Defence Academy of Japan, Yokosuka, Kanagawa, Japan.

INTRODUCTION

Consideration of the deformation and fracture behaviour under high strain rate becomes important in recent evaluation of structural integrity of nuclear power plant. For example, flying objects by tornado, or aircraft impact instruments of nuclear power plants. For the evaluation of such high strain rate events, it is essential to know material properties under high strain rate condition as basic information. However, test methods to obtain such material properties are subjected to the restriction of the strain rate and it is impossible to obtain them only by a single test machine. In this work, deformation and fracture behaviour for various steels in wide range of strain rate are obtained by using several test methods. In addition, the effect of stress triaxiality dependence on the material properties are also investigated.

METHOD

Two ferritic steels (SM400C and STPT410 in JIS Standards) and austenitic steel (SUS304 in JIS Standards) are selected as material. The chemical compositions are shown in Table 1. Tensile tests at the strain rates of 0.001/s, 0.01/s and 0.1/s were performed by normal-speed tensile test machines, those by 1/s, 10/s, and 100/s were performed by hydraulic high-speed tensile test machine (Shimadzu HITS-TX) as shown in Figure 1. The strains rate is defined for gauge length. However, we find that it is better to use distance between grips as reference length to calculate strain from our finite element analysis than the gauge length. Therefore, the resulted strain is smaller than the pre-defined strain rate. Strain rates above 100/s were performed by impact tensile tests using tensile type split Hopkinson bar (SHB) test machine (Ogawa and Sugiyama, 2004) as shown in Figure 2. The SHB test machine consists of 4m length input and output bars made by aluminium alloy. The length and the light material enable to impose big strain to a specimen.

Smooth round-bar and circumferentially notched test pieces, where the stress triaxiality at the notch was higher than 1/3, were used as shown in Figure 2. To unite the shapes of the specimens, brims, which

should not be used in SHB testes, are not made for the specimens. Strain rate of gauge, 0.001/s, 0.01/s, 0.1/s, 1/s, 10/s, and 100/s corresponds to strain rate between grips of 0.00083/s, 0.083/s, 0.83/s, 8.3/s, and 83/s for ferritic steels and that of 0.00071/s, 0.071/s, 0.71/s, 7.1/s, 71/s for SUS304. The diameter of the round bar and the smallest diameter of the notched specimen were both 3mm and the notch radius was 0.5, 1.0 or 1.5mm as shown in Figure 4.

Table 1: Chemical composition of steel materials.

Material	Chemical composition (mass%)						
	C	Si	Mn	P	S	Ni	Cr
SM400C	0.13	0.20	1.03	0.017	0.006		
STPT410	0.20	0.19	0.84	0.016	0.003		
SUS304	0.05	0.40	1.08	0.032	0.005	8.07	18.12

Figure 1. High speed tensile test machine.

Figure 2. Tensile type SHB test machine.

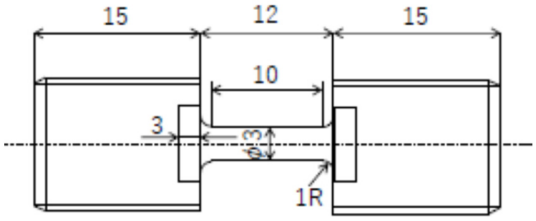

(a) round bar specimen for the ferritic steels

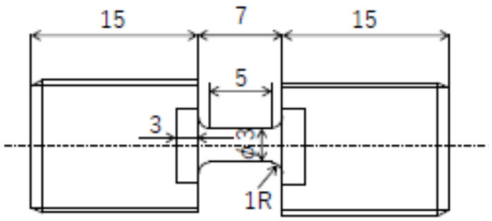

(b)round bar specimen for SUS304

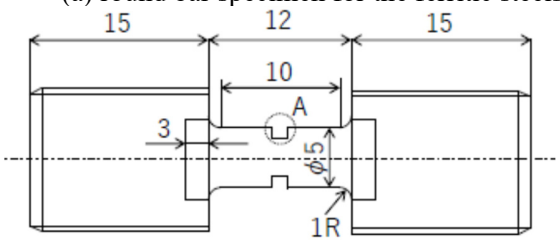

(c) notched bar specimen for ferritic steel

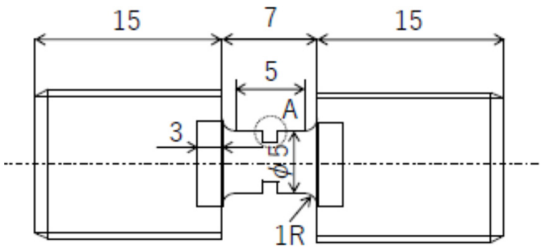

(d)notched round bar specimen for SUS304

Figure 3. Test pieces for normal tensile tests. Units are mm. "A" indicates circumferential notch in Figure 4. It is noted that the grip size depends on a test machine.

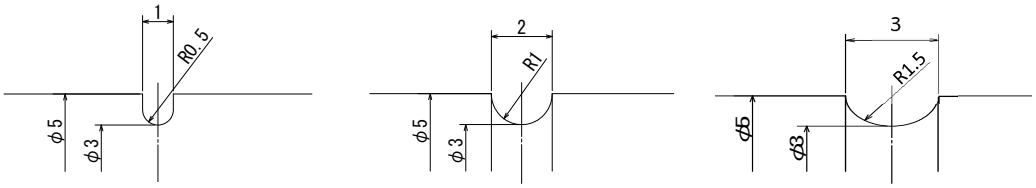

(a)notch radius 0.5mm (b)notch radius 1mm (c)notch radius 1.5mm

Figure 4. Circumferential notches of test pieces

In this work, stress triaxiality, TF is defined as,

$$\mathrm{TF} = \frac{\sigma_1 + \sigma_2 + \sigma_3}{3\sigma_\mathrm{e}}, \tag{1}$$

where σ_i and σ_e are principal stress and equivalent stress, respectively. TF of a circumferentially cracked test piece $\mathrm{TF_{tp}}$ is calculated from Bridgman's equation (Bridgeman, 2013) (as,

$$\mathrm{TF_{tp}} = \frac{1}{3} + \ln\left(1 + \frac{r}{2R}\right), \tag{2}$$

where r is minimum radius of a circumferentially cracked test piece and R is a notch radius. $\mathrm{TF_{tp}}$ of the circumferentially notched test pieces whose R is 0.5, 1.0 and 1.5mm notch results stress triaxiality of 1.25, 0.893, and 0.739, respectively.

Nominal stress σ_n and nominal strain ε_n are transformed into true stress σ_t and true strain ε_t as,

$$\sigma_\mathrm{t} = \sigma_\mathrm{n}(1 + \varepsilon_\mathrm{n}), \tag{3}$$

$$\varepsilon_\mathrm{t} = \ln(1 + \varepsilon_\mathrm{n}). \tag{4}$$

The Johnson-Cook constitutive law (Johnson and Cook, 1985) is used to represent these true stress and strain as,

$$\sigma = \left(A + B\bar{\varepsilon}_p^n\right)\left(1 + C\ln\frac{\dot{\bar{\varepsilon}}_p}{\dot{\bar{\varepsilon}}_0}\right), \tag{5}$$

where A, B, C, and n are material constants, $\bar{\varepsilon}_p$, $\dot{\bar{\varepsilon}}_p$ are $\dot{\bar{\varepsilon}}_0$ equivalent strain, equivalent strain rate and

reference equivalent strain rate. In order to consider yield plateau, the Johnson-Cook constitutive law is extended as,

$$\sigma = \{A + B\langle \bar{\varepsilon}_p - \bar{\varepsilon}_u \rangle^n\}\left(1 + C \ln \frac{\dot{\bar{\varepsilon}}_p}{\dot{\bar{\varepsilon}}_0}\right), \tag{6}$$

where, $\bar{\varepsilon}_u$ is strain at the plateau, and $\langle \cdot \rangle$ is Macaulay bracket.

The strain rates of notched specimens are measured by digital image correlation (DIC) analysis for the high-speed tensile tests and the SHB tests. The test pieces are painted by random patterns and strain is measured by the correlation of the pattern from images recorded by high-speed cameras. MEMRECAM ACS-1 (nac Image Technology, Inc.) was used for the SHB tests as shown in Figure 5. Sample test images are shown in Figure 6. DIC analyses were conducted by GOM Correlate Professional as shown in Figure 7. Basically, 3D-DIC analysis by using two cameras was used to measure deformation in three directions as shown in Figure 5. 2D-DIC analysis was only used for notch radius=0.5mm at high-speed tensile tests where 3D-DIC analysis was impossible due to the narrow notch. It is noted that 3D-DIC analysis enables to measure deformation along depth, however, the measured deformation along depth was very small and 2-DIC analysis can be acceptable. The strain rate during the deformation shows constant trend for the SHB tests and average strain beyond the strain of 1% is considered as strain rate. The strain rate at the notch during the deformation shows constant trend for the SHB tests and average strain beyond the strain of 1% was considered as the strain rate of the notched specimen. The strain rate at the notch during the deformation shows increasing trend for the high-speed tests and average strain from the strain of 5% to 20%, where uniform elongation is assumed, was considered as the strain rate of the notched specimen. The strain rate of normal tensile tests, where DIC analysis was not conducted due to the cost problem, was guessed from relation between the strain rate of the notch and the imposed strain rate of the gauge for the SHB tests and the high-speed tensile tests.

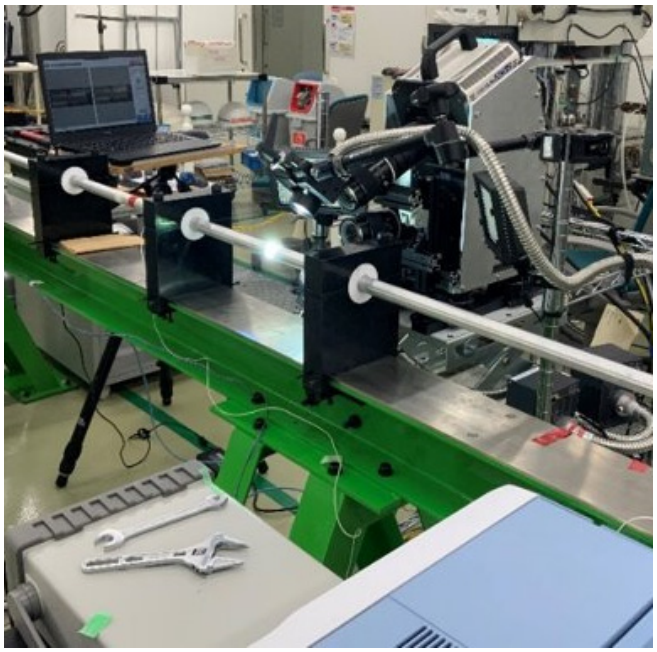

Figure 5. High speed camera for SHB tests (MEMRECAM ACS-1, nac Image Technology, Inc.)

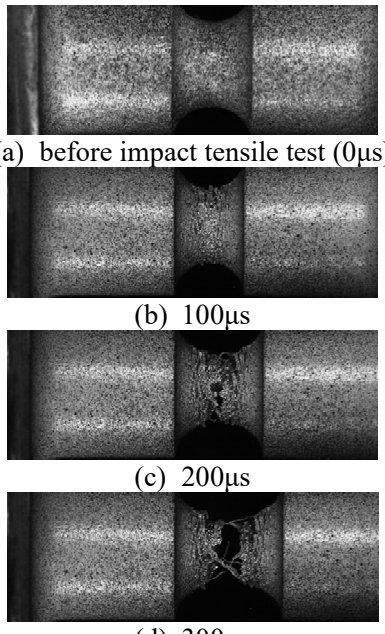

(a) before impact tensile test (0μs)

(b) 100μs

(c) 200μs

(d) 300μs

Figure 6. Sample images of SHB tests by high-speed camera.

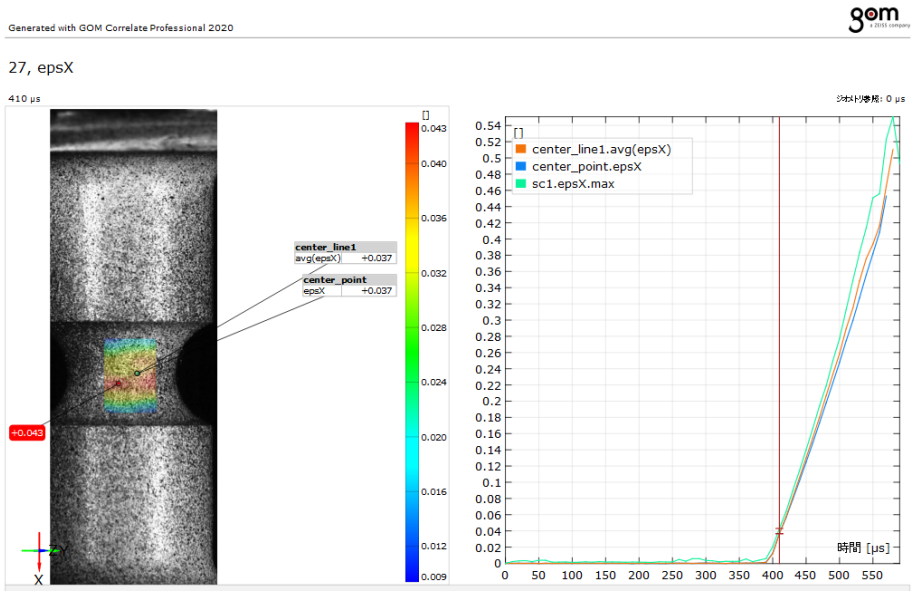

Figure 7. A sample DIC analysis image of a SHB test.

After a tensile test, reduction of area, RA, is calculated as,

$$\mathrm{RA} = 1 - \left(\frac{r_1 + r_2}{2r_0}\right)^2, \tag{7}$$

where, r_1, and r_2 are measured diameters at ruptured surface and r_0 is initial diameter at gauge. From RA, true fracture strain, ε^{f} is calculated as,

$$\varepsilon^f = \ln\left(\frac{1}{1-\mathrm{RA}}\right). \tag{8}$$

RESULTS AND DISCUSSION

From the tensile tests, stress strain (SS) curves of these three types of steels were obtained. The resulted strain rates were around 1000/s for SUS 304 and 500/s for the ferritic steels. The difference in the strain rate came from simply their gauge length, 5mm and 10mm. SS curves obtained by normal and high-speed tensile tests are smooth while those obtained by impact tensile tests are wavy due to spherical wave, which is generated between a specimen and an output bar, as shown in Figures 8 and 9. Yield stress increases as with increasing the imposed strain rate increases as most of other steels. Those suggests those three tensile test methods are consistent. SS curves of two ferritic steels are represented by Johnson-Cook type constitutive law as shown in Figure 8 For the SM400C steel, yield plateau effect is observed and the extended Johnson-Cook low as eq.(6) is used. On the other hand, SS curve of austenitic steel cannot be represented well by Johnson-Cook type constitutive law as shown in Figure 9. In order to represent the SS curve of austenitic steel, we used modified Johnson-Cook type constitutive low in elsewhere (Seo et al., 2022, Seo et al., in press).

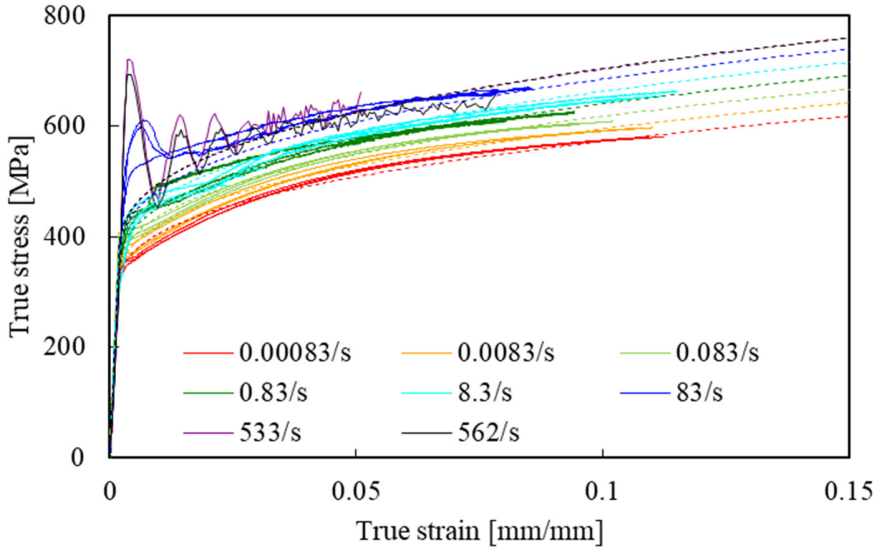

Figure 8. Stress-strain relations of STPT410 (Solid lines and dotted lines indicates expermental values and calculated values by the Johson-Cook law, respectively.)

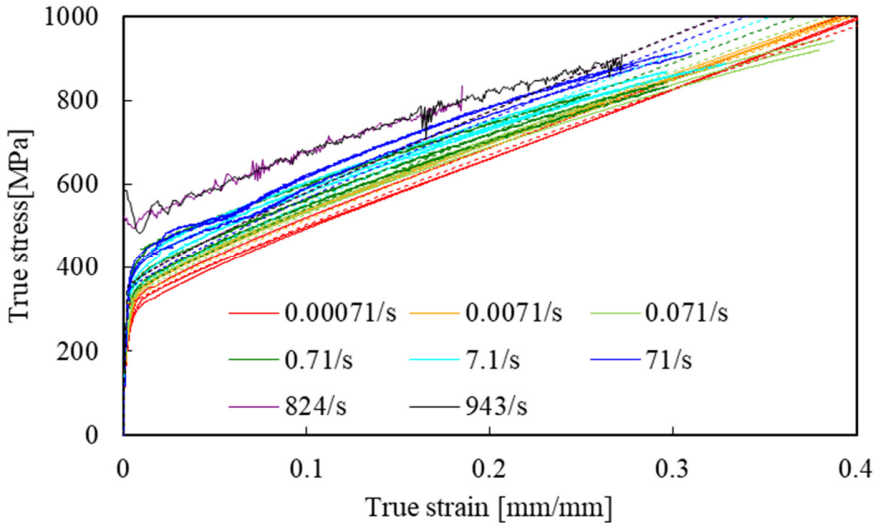

Figure 9. Stress-strain relations of SUS304 (Solid lines and dotted lines indicates expermental values and calculated values by the Johson-Cook law, respectively.)

The stress triaxiality dependence of fracture strain does not depend on strain rate for the ferric carbon steels as shown in Figure 10. The fracture strain is almost constant in the same condition. On the other hand, it depends on strain rate for SUS304 as shown in Figure 11. The fracture strain does not decrease as strain rate increases below the strain rate of 1/s, it drastically decreases around the strain rate of 1/s, and it gradually decreases as strain rate increases beyond the strain rate of 1/s. It is found that the strain rate dependent behaviour is quite different between ferritic steel and austenitic steel. Our X-ray diffraction analysis and electron back scatter diffraction confirmed α' phase only below raptured test pieces which was subjected to strain rate below 1/s. The martensitic transformation makes the volume expansion and reduces RA. It suggests that the strain rate dependence of fracture strain of SUS304 occurred by deformation induced martensitic transformation, which does not occur in high strain rate. This is also a reason not to represent SS curves by the original Johnson-Cook law.

The fracture strain decreases as the stress triaxiality increases for the tested steels. The trends are consistent with conventional stress triaxiality dependent fracture strain models such as Rice and Tracey model (Rice and Tracey, 1969). However, the dependence of the fracture strain tends to be weaker than the models.

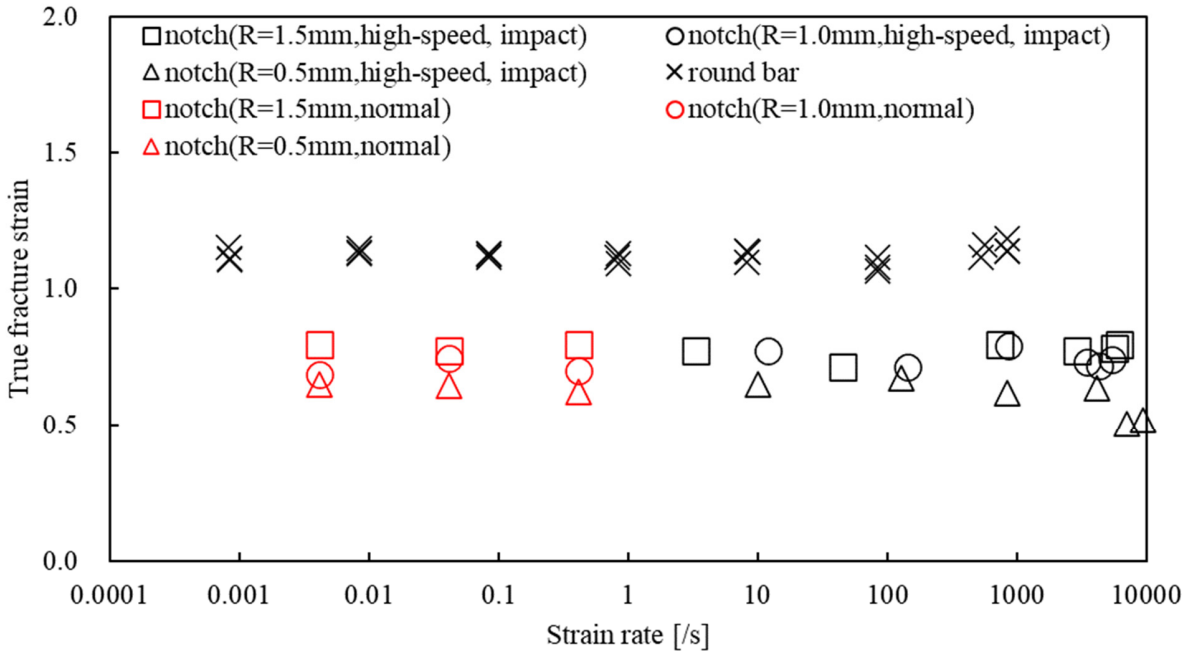

Figure 10. Stress triaxiality dependence of true fracture strain of STPT410 test piece

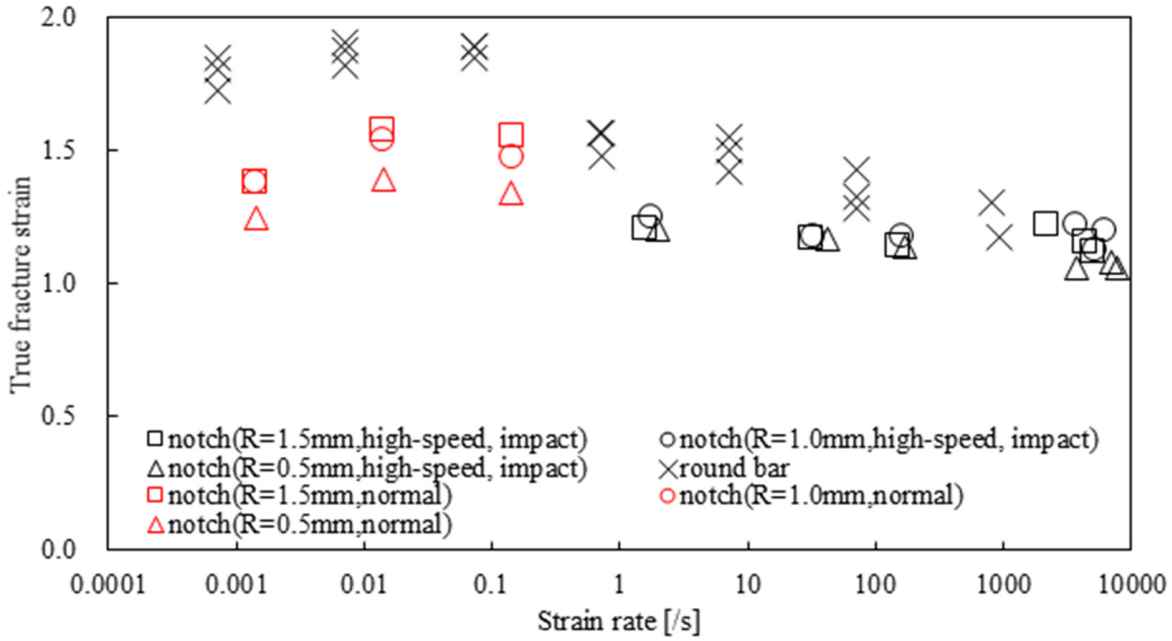

Figure 11. Stress triaxiality dependence of true fracture strain of SUS304 test piece

SUMMARY

In this work, we investigated dependence of SS relations and fracture strains on strain rate, and stress triaxiality of two ferritic carbon steels and one austenitic steel. It is found that the strain rate and stress triaxiality dependence of fracture and deformation properties are quite different between the ferritic steels and the austenitic steel. The temperature dependence of the properties is now investigated and will be presented in the conference.

ACKNOWLEDGEMENTS

The authors thank to Seiichi Ishii and Satoshi Matsumura (nac Image Technology, Inc.) for recording impact tensile tests for DIC analyses and also thank to Soma Watabiki and Kenichi Takane (Kozo Keikaku Engineering Inc.) for DIC analyses for impact tensile tests.

REFERENCES

Ogawa, K. and Sugiyama, F. (2004), “Investigation of Impact Tensile Test Using the Split-Hopkinson Bar”, *Journal of the Society of Materials Scienc*e, Japan, 53(5), 560-565.

Seo, J. M., Jeong, S. S., Kim, Y. J., Kim, J. W., Oh, C. Y., Tokunaga, H., Kumagai, T. and Miura, N. (2022). “Modification of the Johnson-cook Model for the Strain Rate Effect On Tensile Properties of 304/316 Austenitic Stainless Steels.” *Journal of Pressure Vessel Technology*, 144(1), 011501.

Seo, J. M., Kim, H. T., Kim, Y. J, Yamada, H., Kumagai, T., Tokunaga, H., Miura, N., “Effect of strain rate and stress triaxiality on fracture strain of 304 stainless steels for canister impact simulation”, *Nuclear Engineering and Technology* (In press)

Johnson, G. R., and Cook, W. H. (1985). “ Fracture Characteristics of Three Metals Subjected to Various Strains, Strain Rates, Temperatures and Pressures,” *Eng. Fract. Mech.*, 21(1), 31–48.

Bridgman, P. W. (2013). “Studies in large plastic flow and fracture”, Harvard University Press.

Rice, J. R., Tracey, D. M. (1969). “On the ductile enlargement of voids in triaxial stress fields”, *Journal of the Mechanics and Physics of Solids*, 17, 1969, 201–217.